J Mater Sci (2009) 44:2844–2850
DOI 10.1007/s10853-009-3376-0

Correlation among sintering process, porosity, and creep deformation of refractory concrete

Anja Terzić · Ljubica Pavlović

Received: 7 November 2008 / Accepted: 27 February 2009 / Published online: 19 March 2009

Abstract The aim of this paper is to establish the correlation among sintering process, porosity, and important thermo-mechanical property of refractory concrete, i.e., creep. Creep deformation was investigated according to the standard laboratory procedure applied at three temperatures: 1200, 1300, and 1400 °C. Corundum and bauxite-based refractory concretes were investigated. The concretes are varying in chemical and mineralogical composition. Both loss of strength and degradation of material occur when refractory concrete is subjected to increased temperature and compressive static load. Measuring of thermo-mechanical properties can indicate and monitor the changes within microstructure. Variation of refractory concrete microstructure, as a consequence of sintering process, during exposure to constant compressive load and constant elevated temperature during certain time-intervals was investigated using scanning electron microscope and Image Pro Plus program for image analysis. Obtained results of the investigation proved that creep can be useful method when type of refractory concrete is to be chosen for an application.

Introduction

Monolithic elements used for linings of metallurgical furnaces and other plants operating at high temperature, such as linings for oil refinery plants, thermal insulation in plants and in objects, linings in nuclear power plants, linings in chemical and petrochemical industries, and so on, are made of either shaped or unshaped refractory material. Unshaped refractory materials, i.e., refractory concrete, refractory mortar, and shotcrete, have numerous advantages: simplified building of refractory linings, economic aspect, i.e., cheaper process of manufacturing, possibility of damaged lining reparation, and so on [1].

Thermo-mechanical properties, including creep deformation, are among the most important properties of refractory concrete since they can determine its performance in various applications. Creep deformation is measured in terms of applied compressive load in which concrete can withstand at elevated temperature. Microstructure of the material changes when refractory concrete is subjected to compressive load and high temperature: apparent porosity increases, pores become bigger, and cracks within structure open. It results in loss of strength and material degradation. Therefore, development and change of concrete microstructure can be directly monitored by measuring either of these properties. This asumption is also supported with the study by other authors who investigated similar correlation on various refractory materials. For example: Boussuge investigated thermo-mechanical properties on industrial refractories, Kong et al. investigated metakaolin geopolymers exposed to elevated temperatures, Tamtsia et al. investigated early-age short-term creep of hardening cement paste, Wereszczak et al. investigated creep of CaO/SiO2-containing MgO refractories, and so on [2–8].

According to the scientific definition, creep is plastic deformation which is a time-dependent function of an investigated material at constant temperature and constant compressive load (0.2 MPa). Creep takes place at temperatures above $0.5 \cdot T_m$ (T_m is the melting temperature of an investigated material). Creep test can be carried out in

A. Terzić (✉) · L. Pavlović
Institute for Technology of Nuclear and Other Raw Mineral Materials, Franchet d'Esperey 76, 11000 Belgrade, Serbia
e-mail: anja.terzic@gmail.com

different modes (compressive, tensile, and bending). However, creep is generally investigated in compressive mode, because compressive force is the most dominant strain existing in a plant [1, 9].

There are three stages within the creep curve: primary, secondary, and tertiary creeps. Secondary state creep is the dominating region in the creep curve. Therefore, material which is deforming by creep spends the longest period of time in secondary region of creep. During secondary-state creep isothermal sintering process occurs. Rate of creep is always determined by the rate of the slowest diffusion particle movement along the fastest diffusion path [1].

Beside temperature and stress, creep of refractory concrete is affected by the porosity of the material, average grain size, chemical, and mineralogical composition of the refractory concrete, firing temperature of samples and the texture and the microstructure of the material [10–14].

The following equation describes the assumed relationship between a property of the refractory concrete (x) which varies during the sintering process and the duration of the sintering process (t). It is a quantitative description of power-law creep which relates to the isothermal sintering process of refractory concrete during secondary-state creep:

$$x = k \cdot t^n, \tag{1}$$

where k is the time constant, and n is the constant which describes mechanism of sintering.

If variable x is dimensional change (linear shrinkage), then Pines' equation of sintering can be applied [15]:

$$\Delta l/l_0 = k \cdot t^n, \tag{2}$$

where Δl is linear shrinkage of a concrete sample (mm), and l_0 is initial linear dimension of a concrete sample (mm).

The activation energy of the sintering process can be calculated using the following equation:

$$E = (R \cdot T_1 \cdot T_2/(T_1 - T_2)) \cdot \ln(v_1/v_2), \tag{3}$$

where E is activation energy (kJ/mol), R is a gas constant (J/mol °C), T is temperature (°C), v is the rate of sintering process ($v = \Delta l/\Delta t$) (mm/min), Δl is the shrinkage of a sample, and Δt is the duration of shrinkage process.

Besides Eq. 2 suggested by German [16], the other equation which was derived from Frenkel's model of sintering can be used for calculating the activation energy of the sintering process:

$$\Delta l/l_0 = (\sigma \cdot t)/(2 \cdot r \cdot \eta), \tag{4}$$

where σ is the specific surficial energy of boundary grains at the contact, r is the diameter of grains, $\eta = A \cdot \exp(-E/R \cdot T)$ is the viscosity.

Final form of Eq. 4 is:

$$\Delta l/l_0 = c \cdot T^2 \cdot \exp(-E/R \cdot T), \tag{5}$$

where c is the constant that merges all constants from Eq. 4.

If Eq. 5 is to be transformed into its logarithmic form, energy of activation of sintering process could be calculated as the coefficient of the curve slope from the diagram which describes dependence between $\log(\Delta l/l_0) \cdot (1/T^2)$ and $1/T$.

The goal of this study is to use correlation between the results of creep testing and type of sintering process for prediction of behavior and refractory concrete microstructural change during concrete actual service-life.

Experimental

The experiments were performed on two different types of concrete containing different volume fractions and different refractory aggregates. First type of concrete (B sample) contained bauxite as aggregate. Other type of concrete (C sample) was prepared with corundum as aggregate. Aggregates had different granulations (bauxite particle sizes ranging 0–1, 1–4, and 4–6 mm and corundum particle size ranging 0–1, 1–3, and 3–5 mm). Both types of concrete were prepared with high-aluminate cement SECAR 70 (Lafarge). The chemical compositions of the investigated concretes are as follows: sample B (Al_2O_3—62.88%, SiO_2—21.17%, CaO—8.26%) and sample C (Al_2O_3—93.62%, SiO_2—0.7%, CaO—5.97%).

Thermo-mechanical properties of samples C and B were experimentally determined according to standard laboratory procedures [17–20]. Twenty cubic samples (ten for each series) whose dimensions were 10 cm × 10 cm × 10 cm were investigated. After 7 days of curing in climate chamber (at temperature 20 °C), samples were demolded and then dried at 110 °C for 24 h. Afterward samples were transferred into an electric furnace and heated at 1100 °C for 4 h. Such concrete specimens were tested on compressive mechanical strength using conventional laboratory hydraulic pressure device [17].

Creep test was performed on C and B concrete samples (20 and 10 samples, respectively) which were cylindrical; height 50 mm and diameter 50 mm. Hole (diameter 5 mm) was drilled in the center of each concrete sample. Concrete samples were dried at 110 °C for 24 h and afterward preheated at 1100 °C for 4 h. Surface of samples was polished with diamond paste. Pre-heated samples were heated at the rate of 5 °C/min from room temperature (20 °C) up to testing temperature (1200, 1300, or 1400 °C) in the compressive creep apparatus (Netzsch, Germany) and then

submitted to a constant compressive static load (0.2 MPa) at the temperatures of 1200, 1300, and 1400 °C, respectively. Each test on specific temperature lasted for 30 h. During this period secondary-state creep was reached. Investigation was performed according to valid standards [18].

Apparent porosity of the refractory concrete samples was investigated with optical microscope (Olympus, CX31-P) accompanied with PC program for image analysis. The original microscope images were transmitted to the image processor by a color camera. The Image Pro Plus (IPP) program (Materials Pro Analyzer, Version 3.1, Media Cybernetics, Silver Spring, MD, USA) was used in the experiment [21–23]. Results of image analysis were correlated with results of the creep testing.

Same specimens from the creep testing were used in IPP analysis. The specimens were covered with thin chalk-powder film before surface damage was investigated. The film provided better contrast and differentiation of damaged and non-damaged surfaces. Digital photographs of the samples surface were taken before and after each thermal treatment. Different (damaged and non-damaged) surfaces of the samples were marked with different colors using IPP tools. Thus, higher resolution and sharper difference in damaged and non-damaged surfaces on the specimens could be obtained. When the appropriate color is selected, it is possible to quantitatively measure the ratio and level of damaged and non-damaged areas by means of image analysis using a statistical approach.

The images processed in the analyzer were converted into binary form as white features in front of the black background. The binary images were filtered to reduce as much as possible the other features captured together with the target crack images. Then, a final retouching was performed on the images to eliminate the remaining undesirable features and defects by using painting software. In this stage, enhanced images were ready for quantitative analysis. Program contains a procedure for systematic collection of the image analysis data by dividing the total observation area into squares. Following a similar procedure, a transparent grid was attached on each plane section before the analysis. IPP basically works on comparing colors of different objects and calculating squares in marked area. At least ten photographs per sample were analyzed in order to obtain a reliable characterization of the microstructure. The ratio between sample surface area and damaged surface area was calculated for each refractory concrete sample and, thus, surficial apparent porosity was determined.

Results and discussion

Results of the investigation of thermo-mechanical properties are presented in Table 1.

Table 1 Thermo-mechanical properties of concrete samples B and C

Parameter	B	C
Bulk density at 1100 °C (g/cm^3)	2.03	2.46
Water absorption at 1100 °C (%)	15.2	10.1
Refractoriness	20 SK/ 1540 °C	34 SK/ 1755 °C
Refractoriness under compressive load (0.2 MPa)		
T_a (°C)	1300	1500
T_e (°C)	1570	>1600
Compressive strength at 1100 °C (MPa)	16.9	25.3
Apparent porosity at 1100 °C (%)	33.2	27.1

Table 2 Linear creep deformation ($\Delta l/l_0$) of B and C concrete samples after 5 and 30 h of thermal treatment

	$\Delta l/l_0$ at 1200 °C (mm)		$\Delta l/l_0$ at 1300 °C		$\Delta l/l_0$ at 1400 °C	
	B	C	B	C	B	C
After 5 h	−1.86	−2.25	−3.10	−3.24	−4.28	−4.17
After 30 h	−2.57	−2.94	−3.60	−3.72	−4.6	−4.48
$\Delta(\Delta l/l_0)$ (%)	0.71	0.69	0.5	0.48	0.32	0.31

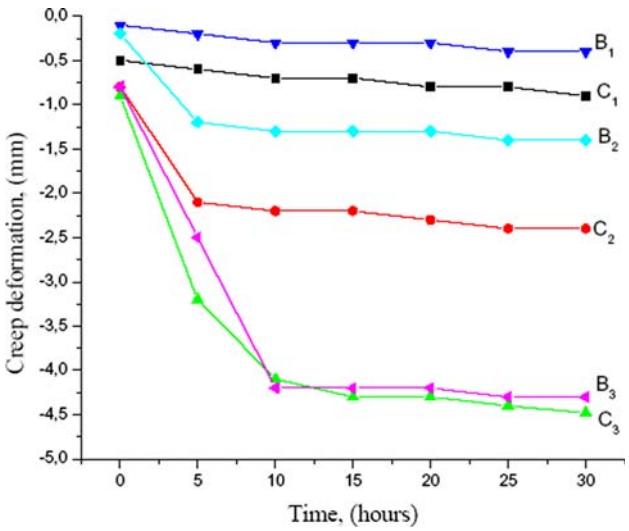

Fig. 1 Creep deformation curves obtained during creep tests on samples B and C at three temperatures: B_1 and C_1—at 1200 °C, B_2 and C_2—at 1300 °C, and B_3 and C_3—at 1400 °C

Results of creep deformation testing are presented in Table 2.

Creep deformation curves of B and C refractory concrete samples are shown in Fig. 1.

The percentage of the compressive creep deformation increases with rising temperature. As it has been noted previously, the creep curve consists of primary, secondary, and tertiary creeps. Secondary-state creep can last for a

long period and it is of prime importance. The analysis of the creep curves of samples B and C (Fig. 1) shows that maximal deformation occurs at temperature 1400 °C for both samples. They are 4.6 and 4.48% for B and C, respectively. Higher percentage of deformation for sample B is consequence of its higher apparent porosity. This statement is also supported with the results of IPP analysis.

Primary creep lasts for 6 h approximately for both samples. Transition of primary into secondary-state creep is hardly noticeable at 1200 °C. However, the transitions at 1300 (after 6 h for B and C) and 1400 °C (after 10 h for B and 15 h for C) are clearly visible. Onset of tertiary-state creep was not detected due to the short interval of investigation (30 h).

The fine matrix situated in inter-aggregate space of concrete sample changes with increasing temperature. Its viscosity significantly diminishes above 1200 °C. Therefore, the plastic deformation of concrete samples at 1400 °C is higher than deformation at 1200 and 1300 °C. The formation of certain amount of liquid phase was noted. Secondary mullite crystallizes from the liquid phase. The amount of mullite depends on Al_2O_3:SiO_2 ratio. Mullite has influence on the deformation at higher temperatures. The creep deformation of the refractory concrete at 1400 °C is higher than deformation at 1200 and 1300 °C due to the surplus of the liquid phase. Ninety percent of the deformation has already taken place at 1400 °C. Rate of deformation significantly decreases in following interval. After 15 h spent at 1400 °C, very little deformation can be observed. Initial deformation is caused by insufficient amount of mullite in structure, whose formation requires sufficient time and high temperatures. Mullite formation induces a structural reinforcement that causes a more rapid mechanical hardening of concrete at high temperatures.

As power-law creep can be applied on creep curves shown in Fig. 1, calculation of sintering constant (n) and activation energy (E) were also performed. Results of dimensional change ($\Delta l/l_0$) of samples B and C were obtained during creep test at 1200, 1300, and 1400 °C. The durations of the dimensional change (shrinkage) of concrete samples were registered by an automatic writer for each time interval. Using Eqs. 2 and 5 approximate sintering constant, i.e., coefficient of sintering reaction mechanism (n) and activation energy (E) has been calculated. The sintering rates and temperature dependences were calculated using coefficient of direction (slope) of the function $\Delta l = f(\Delta t)$. Figure 2 shows numeric results for coefficient of reaction mechanism of sintering process (n) and the rate of sintering (v) for the B and C concretes at temperatures 1200, 1300, and 1400 °C, and also gives conclusion concerning type of sintering mechanism which occurs during secondary-state creep.

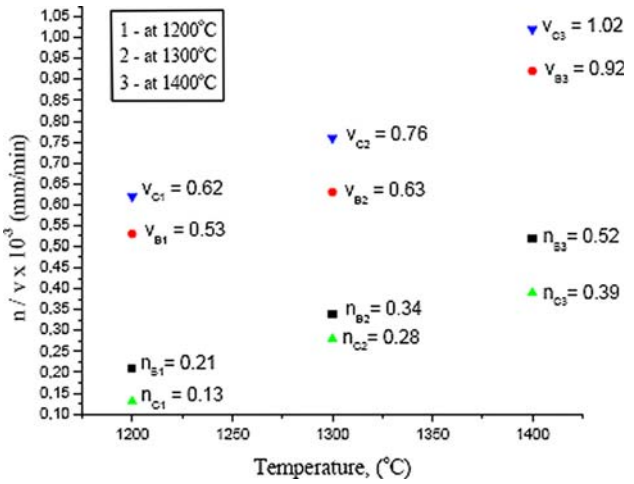

Fig. 2 Results for coefficient of sintering (n), rate of sintering (v), and mechanism of reaction for samples B and C: B_1—surficial diffusion, B_2—diffusion along the grain boundary, B_3—plastic-viscous flow, C_1—surficial diffusion, C_2—surficial diffusion, and C_3—diffusion along the grain boundary

The coefficient n describes the mechanism of particle transport during sintering process in secondary-state creep. From results exposed in Fig. 2 it can be seen that the most dominant mechanisms are: the surficial diffusion, diffusion along grain boundary, and plastic-viscous flow.

Approximate activation energy (E) was calculated using Eq. 3 from results obtained at 1300 °C. Results are presented in Table 3.

The microstructure of concretes was examined using scanning electron microscopy (SEM). SEM (SEM JEOL JSM-5300) photomicrographs of refractory concrete samples heat treated at 1100 °C are shown in Figs. 3 and 4. Aggregate particles sizing few millimeters which are surrounded with fine matrix composed of micronic size particles can be seen in Figs. 3 and 4. Also, there can be seen pores of various sizes. Porosity of these samples was calculated using IPP method and (average) results are: 33.2 and 27.1% for samples B and C, respectively, measured at 1100 °C. Higher porosity of sample B is the reason why its creep deformation is also higher than in the case of sample C, as it was previously assumed (Fig. 1).

By using IPP method, parameters such as maximal, minimal, and average pore diameter (D_{max}, D_{min}, and D_{av}), pore roundness (R), and number (N) of pores within superficial pores were obtained. Digital photos (as explained in section "Experimental") of concrete samples

Table 3 Approximate activation energy (E) for B and C concrete

T (°C)	E_B (kJ/mol)	E_C (kJ/mol)
1200–1300	89.2	84.5
1300–1400	76.9	82.1

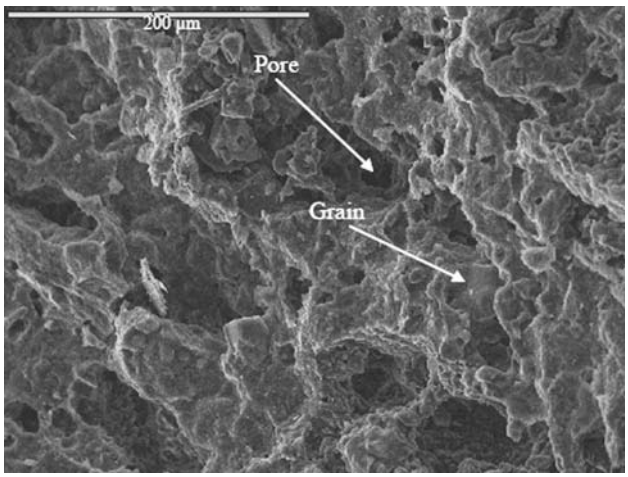

Fig. 3 SEM of B refractory concrete sample heat treated at 1100 °C: porosity is clearly visible and obviously higher than in the case of sample C (Fig. 4)

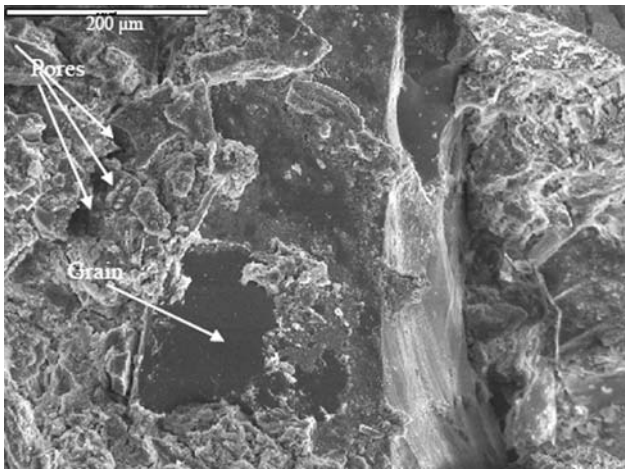

Fig. 4 SEM of C refractory concrete heat treated at 1100 °C: large corundum grains surrounded with matrix are visible

were used in analysis. Results are presented in Table 4. According to IPP analysis, average pore diameter increases untill temperature of approximately 1300 °C is reached and afterward significant shrinkage occurs. Shinkage of pores is a concequence of sintering process. Sample B has smaller average pore diameter although its apparent porosity is higher on all temperatures of investigation. It is consequence of better choice of aggregate granulation. Ideal roundness would be 1.00, and for investigated pores roundness is 1.05–1.15. That means that pores are almost spheric. N is smaller for sample C, which also indicates that apparent porosity of C concrete is smaller than in the case of B concrete, i.e., most of pores are surficial (Table 4).

Microstructure of samples used in creep tests at various temperatures is presented in Figs. 5a–c and 6a–c. Samples heated at 1200 °C (Figs. 5a and 6a) exhibit little structural change when compared to the samples heat treated at 1100 °C. Structural changes are noticeable on the samples exposed to 1300 °C. There can be noticed a formation of liquid phase and emersion of initially formed crystals. The microstructures of samples investigated at 1400 °C are significantly different than the microstructure of the rest of samples. Formation of mullite is noticed in the structure. Mullite provides structural reinforcement and makes the rate of the creep slower (rate of deformation). Larger amount of secondary mullite is noticed in sample B, and it can explain the smaller deformation of these samples during secondary-state creep, when compared with concrete C. Phase analyses confirmed the presence of mullite in concrete samples. Beside previously mentioned, there is significant difference in porosity. Namely, samples of bauxite concrete have noticeably higher porosity than concrete with corundum.

Conclusion

Investigation of time-dependent viscoplastic deformation at various constant temperatures and constant static loads, i.e., creep deformation, lead to the following conclusions: corundum-based concrete samples show smaller deformation than bauxite-based concrete samples investigated at same temperature (1200, 1300, and 1400 °C). Therefore corundum-based concrete is more adequate for application in certain proposed extreme conditions in plants operating at high temperatures. At these temperatures, material is in the secondary-state creep which is a characteristic for most of concrete actual "life" in actual service. Deformation of concrete which occurs at high temperature could damage the plant's lining. However, a structural reinforcement occurs within concrete at temperatures above 1300 °C due to the formation of secondary mullite situated in inter-aggregate space, which was noted by SEM technique. This affects creep and decreases rate of plastic deformation as it is proved in the case of isothermal sintering at 1400 °C for 30 h. Furthermore, this affects all mechanical properties of refractory concrete (mechanical strength and refractoriness are increased, porosity decreased, etc.) and "life" of refractory concrete lining is elongated.

Microstructure of refractory composites was also investigated in this article. Apparent porosity, pore distribution, and pore size of concrete samples were investigated using IPP program. Results presented in this article contribute to the idea of including other test methods for investigation of mechanical properties and microstructure such as nondestructive methods instead of commonly used standard laboratory procedures. Benefits from using image analysis are numerous: it is nondestructive, simple, and fast method; same samples could be used for further tests; there

Table 4 Results of IPP analysis for C and B concrete samples

T (°C)	C					B				
	D_{max} (mm)	D_{min} (mm)	D_{av} (mm)	N	R	D_{max} (mm)	D_{min} (mm)	D_{av} (mm)	N	R
110	0.046	0.0042	0.0067	9	1.08	0.056	0.00129	0.003	51	1.07
1100	0.057	0.00448	0.0077	14	1.1	0.073	0.00137	0.0035	74	1.12
1200	0.072	0.0045	0.0084	22	1.13	0.079	0.00138	0.0037	81	1.14
1300	0.089	0.0046	0.0089	26	1.138	0.085	0.00138	0.004	80	1.22
1400	0.084	0.00455	0.0086	24	1.091	0.082	0.00130	0.0038	75	1.17

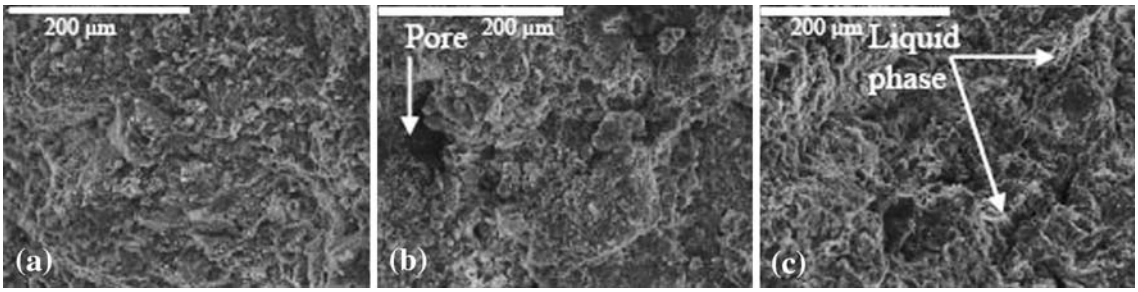

Fig. 5 SEM of sample B heat treated at: **a** 1200 °C; **b** 1300 °C; **c** 1400 °C: pores within sample B are bigger; and emersion of liquid phase can be seen (*white shade* on SEM microphotograph)

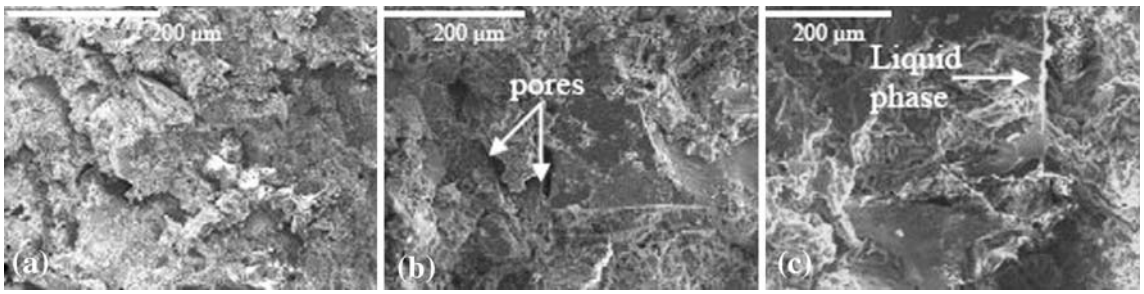

Fig. 6 SEM of sample C heat treated at: **a** 1200 °C; **b** 1300 °C; **c** 1400 °C: pores are visibly smaller than in sample B; liquid phase is noticeable

is financial benefit in minimizing number of samples for testing—there is saving in material and in time; entirely new and important information about damages and porosity of surface could be obtained—precise diameters of pores, roundness, number of pores in a section, and so on; as surficial damage level is measured, results could be useful for prediction of sample behavior during further testing or application.

Investigations presented in this article confirmed that results of creep deformation test, image analysis, and quantitative description of sintering process are interconnected and that they, as well their interconnection, can be useful when type of refractory concrete is to be chosen for application in a metallurgical furnace or some other plant operating at high temperature.

Acknowledgement This study has been supported by Serbian Ministry of Science under Project nos. 19012 and 16004.

References

1. Bazant Z, Kaplan MF (1996) Concrete at high temperatures, material properties and mathematical models, concrete design and construction series. Longmann Group, London
2. Boussuge M (2008) J Mater Sci 43(12):4069. doi:10.1007/s10853-008-2534-0
3. Kong DLY, Sanjayan JG, Sagoe-Crentsil K (2008) J Mater Sci 43(3):824. doi:10.1007/s10853-007-2205-6
4. Tam VWY, Tam CM (2007) J Mater Sci 42(10):3592. doi:10.1007/s10853-006-0379-y
5. Tamtsia BT, Beaudoin JJ, Marchand J (2003) J Mater Sci 38(10):2247. doi:10.1023/A:1023769323629
6. Chung DDL (2002) J Mater Sci 37(4):673. doi:10.1023/A:1013889725971
7. Wereszczak AA, Kirkland TP, Curtis WF (1999) J Mater Sci 34(2):215. doi:10.1023/A:1004427314573
8. Posarac M, Dimitrijevic M, Volkov-Husovic T, Devecerski A, Matovic B (2008) J Eur Ceram Soc 28:1275
9. Sinonin LLF, Olgonon C, Maximilien S, Fantozzi G (2000) J Am Ceram Soc 83:81

10. Altun IA (2001) Cem Concr Res 31:1233–1239
11. Cardoso F, Innocentini M, Miranda M, Valenzuela F, Pandolfelli V (2004) J Eur Ceram Soc 24:797
12. Zawrah M, Khalil NM (2001) Ceram Int 27:689
13. Hipedinger N, Scian A, Aglietti E (2004) Cem Concr Res 34:157
14. Karadeniz E, Gurcan C, Ozgen S, Aydin S (2007) J Eur Ceram Soc 27:1849
15. Prassas M, Phalippou J, Zarzycki J (1996) Science of ceramic processing. Wiley-Interscience Publication, New York
16. German RM (1996) Sintering theory and practice. Wiley-Interscience Publication, New York
17. Standard: JUS B. D8. 304
18. Standard JUS B. D8. 303
19. Standard JUS B. D8. 301
20. Standard JUS B. D8. 312
21. Boccaccini DN, Canio M, Volkov Husovic T (2007) J Mater Sci 43(12):4079. doi:10.1007/s10853-007-2315-1
22. Volkov Husovic T, Jancic R, Mitrakovic D (2005) Am Ceram Soc Bull 84(10):1
23. Volkov T, Jancic R, Mitrakovic D (2005) Mater Sci Forum 492–493:561